Eur. Phys. J. Plus (2015) **130**: 227
DOI 10.1140/epjp/i2015-15227-9

THE EUROPEAN PHYSICAL JOURNAL PLUS

Regular Article

Quantum statistical characteristics of the interaction between two two-level atoms and radiation field

M. Sebawe Abdalla[1,a], E.M. Khalil[2,3], A.S.-F. Obada[3], J. Peřina[4], and J. Křepelka[5]

[1] Mathematics Department, College of Science, King Saud University, P.O. Box 2455, Riyadh 11451, Saudi Arabia
[2] Mathematics Department, Faculty of Science, Taif University, P.O. Box 888 Taif 21974, Saudi Arabia
[3] Mathematics Department, Faculty of Science, Al-Azhar University, Nasr City 11884, Cairo, Egypt
[4] Department of Optics and Joint Laboratory of Optics of Palacký University and Institute of Physics of AS CR, Faculty of Science, Palacký University, 17. listopadu 12, 771 46 Olomouc, Czech Republic
[5] Joint Laboratory of Optics of Palacký University and Institute of Physics of Physics of Academy of Sciences of the Czech Republic, 17. listopadu 50a, 771 46 Olomouc, Czech Republic

Received: 12 February 2015 / Revised: 23 September 2015
Published online: 12 November 2015

Abstract. A quantum optics model is considered where the cavity field interacts with two coupled atoms. The time-dependent wave function is obtained and used to derive the density matrix from which we discussed some statistical properties for the present system. The atom-atom entanglement, atoms-cavity entanglement, entropy and variance squeezing, the Pegg-Barrnet phase and the fidelity are discussed with the effects of the initial conditions, atom-atom coupling and the detuning parameter displayed. It is shown that an increase in the value of the atom-atom coupling parameter leads to an increase in the degree of entanglement. Numerical results show that under some conditions the phenomena of entanglement and the collapses and the revivals emerge. Nonclassical properties are demonstrated by means of the field quantum statistical characteristics, such as photon-number distribution, Husimi, Wigner and Glauber-Sudarshan quasidistributions and the corresponding variances.

1 Introduction

Entanglement plays a basic role in quantum computation and quantum communication [1,2]. Therefore one of the particular interesting schemes, in which entanglement can be created, is a system containing two two-level atoms, since they can represent two qubits, as building blocks of the quantum gates that are essential to implement quantum protocols in quantum information processing. Two-atom entangled states have been demonstrated experimentally using ultra cold trap ions [3,4] and cavity quantum electrodynamics schemes [5]. The Tavis-Cummings model [6] can be used to understand the dynamics of entanglement for atoms interacting with quantum electromagnetic field. The two-atom Tavis-Cummings model describes the simplest fundamental interaction between a single mode of quantized electromagnetic field and two atoms under the usual two-level and rotating-wave approximations [7]. The atom-field entanglement for two two-level atoms interacting with coherent cavity field by means of one-photon transitions has been studied in [8,9]. The important generalization of the considered model is the two-atom two-photon Tavis-Cummings model. Two-photon transitions in atomic systems play an important role because of the high degree of correlation between emitted photons. The interest in the investigation of the two-photon models is stimulated by the experimental realization of a two-photon one-atom micromaser on Rydberg transitions in a microwave cavity [10]. The atom-field entanglement for the two-atom Tavis-Cummings model has been investigated for nondegenerate, Raman and degenerate two-photon transitions in [11,12]. The effects of Stark shift on the purity loss of the two-atom multi-photon system and different partitions of the system (field-two-atom, atom-(field + atom)) have been considered in [13].

It is important to study the entanglement properties in realistic physical system, where the subsystem of our interest, two-qubit subsystem, interacts with other subsystems as the environment of the two-qubit subsystem. This type of interaction causes the indirect coupling between the two qubits. The entanglement between qubits and an environment unavoidably causes decoherence of qubits, one of the biggest obstacles in quantum information processing.

[a] e-mail: m.sebaweh@physics.org

It has been believed that qubits should be isolated from environment. However, it has been shown that two qubits which do not interact directly with each other but interact with the environment can be entangled or disentangled [14–17]. In addition to the indirect coupling with each other, there is another type of two-qubit direct coupling, such as dipole coupling in NMR [18] or Coulomb coupling in superconducting charge qubits [19].

On the other hand, a thorough understanding of entanglement dynamical evolution in quantum physical systems, such as quantum optics systems, has obvious implications for quantum information processing, as well as for understanding fundamental quantum mechanics. Vast efforts have been devoted to studying bipartite entanglement dynamics in the one-atom model [20–23] and two-atom model [24]. However, the atom-atom coupling was not taken into account. Here we consider the atom-atom coupling and focus on the mediating roles of the atom-cavity indirect coupling and atom-atom direct coupling by studying the evolution of different phenomena related to the considered system.

Our interest lies in the case where the atom-atom coupling is included. In the dipole and rotating-wave approximations, the system Hamiltonian of the whole system reads

$$\frac{\hat{H}}{\hbar} = \omega\hat{a}^\dagger\hat{a} + \sum_{j=1}^{2}\Omega_j\hat{\sigma}_z^{(j)} + \sum_{j=1}^{2}\lambda_1\left(\hat{a}\hat{\sigma}_+^{(j)} + \hat{a}^\dagger\hat{\sigma}_-^{(j)}\right) + \mathrm{i}\lambda_2\left(\hat{\sigma}_+^{(1)}\hat{\sigma}_-^{(2)} - \hat{\sigma}_-^{(1)}\hat{\sigma}_+^{(2)}\right), \tag{1}$$

where $\hat{a}^\dagger$ and $\hat{a}$ are the creation and annihilation operators for the cavity mode such that $[\hat{a}, \hat{a}^\dagger] = 1$ and ω and $\Omega_j, j = 1, 2$ are the field and the atomic transition frequencies, respectively, while λ_1 is the coupling constant between the field and each of the atoms and λ_2 between the two atoms themselves. The operators $\hat{\sigma}_+^{(j)}(\hat{\sigma}_-^{(j)})$ and $\hat{\sigma}_z^{(j)}$ $(j = 1, 2)$ are the usual raising (lowering) and inversion operators for the two-level atomic system, satisfying the commutation relations

$$[\hat{\sigma}_z^{(j)}, \hat{\sigma}_\pm^{(j)}] = \pm 2\hat{\sigma}_\pm^{(j)}, \quad [\hat{\sigma}_+^{(i)}, \hat{\sigma}_-^{(j)}] = \hat{\sigma}_z^{(j)}\delta_{ij}. \tag{2}$$

In this context we may refer to the last part of the present paper, where we will demonstrate nonclassical properties of this system using field statistical characteristics, such as photon-number distribution, Husimi, Wigner and Glauber-Sudarshan quasidistributions and the corresponding variances, related to antinormal, symmetric and normal operator ordering. Particular attention is devoted to the examination of the nonclassical properties of the system.

From the above, as one can see, the problem would be much easier and the chance to find the dynamical operators or the wave function becomes more tractable than for the nonconservative case. However, the existence of the atom-atom interaction leads to some complications. This is solved in the forthcoming section where an exact solution of the wave function in the Schrödinger picture is obtained. This is followed by a discussion of the linear entropy of the atomic state in sect. 3. In sect. 4 we consider the atomic inversion where we discuss the influence of the detuning and the atom-atom interaction on the behavior of the revivals and collapses phenomenon. The entropy squeezing and variance squeezing phenomena are also considered in sect. 5. Pegg-Barnett phase and fidelity are discussed in sect. 6 and sect. 7, respectively. In sect. 8 the characteristics of the field are introduced and we illustrate the results of the last part of the paper in sect. 9. Finally we give our conclusion in sect. 10.

2 Analytical solution

To discuss the statistical properties of the present system we have to obtain the solution of the wave function in the Schrödinger picture or to find the dynamical operators by solving the Heisenberg equations of motion. We write the Heisenberg equations of motion for the operators $\hat{n} = \hat{a}^\dagger\hat{a}$ and $\hat{\sigma}_z^{(j)}$ $(j = 1, 2)$ in what follows:

$$\begin{aligned}
\frac{\mathrm{d}\hat{n}}{\mathrm{d}t} &= -\mathrm{i}\sum_{j=1}^{2}\lambda_1\left(\hat{a}\hat{\sigma}_+^{(j)} - \hat{a}^\dagger\hat{\sigma}_-^{(j)}\right),\\
\frac{\mathrm{d}\hat{\sigma}_z^{(1)}}{\mathrm{d}t} &= 2\mathrm{i}\lambda_1\left(\hat{a}\hat{\sigma}_+^{(1)} - \hat{a}^\dagger\hat{\sigma}_-^{(1)}\right) - 2\lambda_2\left(\hat{\sigma}_+^{(1)}\hat{\sigma}_-^{(2)} + \hat{\sigma}_-^{(1)}\hat{\sigma}_+^{(2)}\right),\\
\frac{\mathrm{d}\hat{\sigma}_z^{(2)}}{\mathrm{d}t} &= 2\mathrm{i}\lambda_1\left(\hat{a}\hat{\sigma}_+^{(2)} - \hat{a}^\dagger\hat{\sigma}_-^{(2)}\right) + 2\lambda_2\left(\hat{\sigma}_+^{(1)}\hat{\sigma}_-^{(2)} + \hat{\sigma}_-^{(1)}\hat{\sigma}_+^{(2)}\right),
\end{aligned} \tag{3}$$

from which we can show that the operator

$$\hat{N} = \hat{n} + \frac{1}{2}\sum_{j=1}^{2}\hat{\sigma}_z^{(j)}, \tag{4}$$

is a constant of motion. Using this fact the Hamiltonian model (1) can written in the form

$$\frac{\hat{H}}{\hbar} = \omega\hat{N} + \hat{C}, \tag{5}$$

where the operator $\hat{C}$ is given by

$$\hat{C} = \sum_{j=1}^{2}\left[\frac{\delta_j}{2}\hat{\sigma}_z^{(j)} + \lambda_1\left(\hat{a}\hat{\sigma}_+^{(j)} + \hat{a}^\dagger\hat{\sigma}_-^{(j)}\right)\right] + \mathrm{i}\lambda_2\left(\hat{\sigma}_+^{(1)}\hat{\sigma}_-^{(2)} - \hat{\sigma}_-^{(1)}\hat{\sigma}_+^{(2)}\right). \tag{6}$$

In the above relation the quantities δ_1 and δ_2 are the detuning parameters defined by

$$\delta_j = 2\Omega_j - \omega, \quad j = 1, 2. \tag{7}$$

It is an easy task to show that the operators $\hat{N}$ and $\hat{C}$ commute and consequently each of them commutes with the Hamiltonian $\hat{H}$. Since the Hamiltonian is a constant of motion, then the operator $\hat{C}$ is also a constant of motion. We now assume that the field is initially in the coherent state and the atoms are identical and initially in pure atomic states. In this case the wave function of the atoms-field system at $t = 0$ can be written as

$$|\psi(0)\rangle = [c_1|+\rangle_1|+\rangle_2 + c_2|+\rangle_1|-\rangle_2 + c_3|-\rangle_1|+\rangle_2 + c_4|-\rangle_1|-\rangle_2] \otimes |\alpha\rangle, \tag{8}$$

where $|\alpha\rangle$ is the coherent state given by

$$|\alpha\rangle = \sum_{n=0}^{\infty} Q_n|n\rangle, \quad Q_n = \frac{\alpha^n}{\sqrt{n!}}\exp\left(-\frac{|\alpha|^2}{2}\right), \tag{9}$$

$|+\rangle_i$ and $|-\rangle_i$ are the upper and lower states of the i-th atom and c_i, $i = 1, 2, 3, 4$ are arbitrary complex quantities that satisfy the condition

$$|c_1|^2 + |c_2|^2 + |c_3|^2 + |c_4|^2 = 1. \tag{10}$$

In what follows we assume that the condition for the two atoms in exact resonance case is fulfilled, which means that $\delta_1 + \delta_2 = 0$. The wave function $|\psi(t)\rangle$ at the time $t > 0$ takes the form

$$\begin{aligned}|\psi(t)\rangle = \sum_{n=0}^{\infty}&\left(X_1(n,t)|+\rangle_1|+\rangle_2|n\rangle + X_2(n,t)|+\rangle_1|-\rangle_2|n+1\rangle\right.\\ &\left.+X_3(n,t)|-\rangle_1|+\rangle_2|n+1\rangle + X_4(n,t)|-\rangle_1|-\rangle_2|n+2\rangle\right).\end{aligned} \tag{11}$$

The coefficients $X_j(n,t)$, $j = 1, 2, 3, 4$ are obtained by solving the Schrödinger equation $\mathrm{i}\hbar\partial|\psi(t)\rangle/\partial t = \hat{H}|\psi(t)\rangle$, where $\hat{H}$ is given by eq. (5). Considering that the first part gives a phase component, we concentrate on the second part, *i.e.* on the interaction picture. In this case, for $\delta_1 + \delta_2 = 0$, we obtain the following system of the differential equations for $X_j(n,t)$:

$$\begin{aligned}\frac{\mathrm{d}X_1}{\mathrm{d}t} &= -\mathrm{i}\nu_1(n)(X_2 + X_3),\\ \frac{\mathrm{d}X_2}{\mathrm{d}t} &= -\mathrm{i}\ \delta_1 X_2 + \lambda_2 X_3 - \mathrm{i}\nu_1(n)X_1 - \mathrm{i}\nu_2(n)X_4,\\ \frac{\mathrm{d}X_3}{\mathrm{d}t} &= \mathrm{i}\delta_1 X_3 - \lambda_2 X_2 - \mathrm{i}\nu_1(n)X_1 - \mathrm{i}\nu_2(n)X_4,\\ \frac{\mathrm{d}X_4}{\mathrm{d}t} &= -\mathrm{i}\nu_2(n)(X_2 + X_3),\end{aligned} \tag{12}$$

where

$$\nu_1(n) = \lambda_1\sqrt{n+1}, \quad \nu_2(n) = \lambda_1\sqrt{n+2}. \tag{13}$$

After straightforward calculations, we find that the time-dependent coefficients $X_j(n,t)$, $j = 1, 2, 3, 4$ are given by

$$X_j(n,t) = \sum_{i=1}^{4} A_{ji}(n,t), \tag{14}$$

where

$$
\begin{aligned}
A_{11}(n,t) &= c_1 Q_n \left[\frac{\mu_1^2(n) - 2\nu_1^2(n)(1-\cos\mu_1(n)t)}{\mu_1^2(n)}\right],\\
A_{12}(n,t) &= -c_2 Q_{n+2}\left[\frac{\delta^*\nu_1(n)(1-\cos\mu_1(n)t)}{\mu_1^2(n)} + \mathrm{i}\frac{\nu_1(n)\sin\mu_1(n)t}{\mu_1(n)}\right],\\
A_{13}(n,t) &= c_3 Q_{n+2}\left[\frac{\delta^*\nu_1(n)(1-\cos\mu_1(n)t)}{\mu_1^2(n)} - \mathrm{i}\frac{\nu_1(n)\sin\mu_1(n)t}{\mu_1(n)}\right],\\
A_{14}(n,t) &= -c_4 Q_{n+4}\frac{2\nu_1(n)\nu_2(n)(1-\cos\mu_1(n)t)}{\mu_1^2(n)},\\
A_{21}(n,t) &= -c_1 Q_n\left[\frac{\delta\nu_1(n)(1-\cos\mu_1(n)t)}{\mu_1^2(n)} + \mathrm{i}\frac{\nu_1(n)\sin\mu_1(n)t}{\mu_1(n)}\right],\\
A_{22}(n,t) &= c_2 Q_{n+2}\left[\frac{\mu_1^2(n) - \mu_2^2(n)(1-\cos\mu_1(n)t)}{\mu_1^2(n)} - \mathrm{i}\frac{\delta_1\sin\mu_1(n)t}{\mu_1(n)}\right],\\
A_{23}(n,t) &= -c_3 Q_{n+2}\left[\frac{\mu_3^2(n)(1-\cos\mu_1(n)t)}{\mu_1^2(n)} + \frac{\lambda_2\sin\mu_1(n)t}{\mu_1(n)}\right],\\
A_{24}(n,t) &= -c_4 Q_{n+4}\left[\frac{\delta\nu_2(n)(1-\cos\mu_1(n)t)}{\mu_1^2(n)} + \mathrm{i}\frac{\nu_2(n)\sin\mu_1(n)t}{\mu_1(n)}\right],\\
A_{31}(n,t) &= c_1 Q_n\left[\frac{\delta\nu_1(n)(1-\cos\mu_1(n)t)}{\mu_1^2(n)} - \mathrm{i}\frac{\nu_1(n)\sin\mu_1(n)t}{\mu_1(n)}\right],\\
A_{32}(n,t) &= -c_2 Q_{n+2}\left[\frac{\mu_3^2(n)(1-\cos\mu_1(n)t)}{\mu_1^2(n)} + \frac{\lambda_2\sin\mu_1(n)t}{\mu_1(n)}\right],\\
A_{33}(n,t) &= c_3 Q_{n+2}\left[\frac{\mu_1^2(n) - \mu_2^2(n)(1-\cos\mu_1(n)t)}{\mu_1^2(n)} + \mathrm{i}\frac{\delta_1\sin\mu_1(n)t}{\mu_1(n)}\right],\\
A_{34}(n,t) &= c_4 Q_{n+4}\left[\frac{\delta\nu_2(n)(1-\cos\mu_1(n)t)}{\mu_1^2(n)} - \mathrm{i}\frac{\nu_2(n)\sin\mu_1(n)t}{\mu_1(n)}\right],\\
A_{41}(n,t) &= -c_1 Q_n\frac{2\nu_1(n)\nu_2(n)(1-\cos\mu_1(n)t)}{\mu_1^2(n)},\\
A_{42}(n,t) &= -c_2 Q_{n+2}\left[\frac{\delta^*\nu_2(n)(1-\cos\mu_1(n)t)}{\mu_1^2(n)} + \mathrm{i}\frac{\nu_2(n)\sin\mu_1(n)t}{\mu_1(n)}\right],\\
A_{43}(n,t) &= c_3 Q_{n+2}\left[\frac{\delta^*\nu_2(n)(1-\cos\mu_1(n)t)}{\mu_1^2(n)} - \mathrm{i}\frac{\nu_2(n)\sin\mu_1(n)t}{\mu_1(n)}\right],\\
A_{44}(n,t) &= c_4 Q_{n+4}\left[\frac{\mu_1^2(n) - 2(\nu_2(n))^2(1-\cos\mu_1(n)t)}{\mu_1^2(n)}\right],
\end{aligned}
\tag{15}
$$

where

$$
\begin{aligned}
\mu_1(n) &= \sqrt{|\delta|^2 + 2\,(\nu_1^2(n) + \nu_2^2(n))},\\
\mu_2(n) &= \sqrt{|\delta|^2 + (\nu_1^2(n) + \nu_2^2(n))},\\
\mu_3(n) &= \sqrt{\nu_1^2(n) + \nu_2^2(n)},\\
\delta &= \delta_1 + \mathrm{i}\lambda_2.
\end{aligned}
\tag{16}
$$

Note the dependence of the arguments of the trigonometric functions on $\mu_1(n)$. Now if one uses the state $|\psi(t)\rangle$ given by eq. (11), then the reduced atomic density matrix can be constructed from tracing the expression $\hat{\rho} = |\psi(t)\rangle\langle\psi(t)|$ over the field variables. Thus having obtained the exact expression for the wave function, we are able to obtain the accurate statements for the atoms-field entanglement parameter and consequently the degree of the entanglement.

3 Linear entropy

In recent years, various research works have in quantum entanglement, which is one of the main parts for the execution of quantum information processing devices [25]. From the obtained results in the previous section, we may come to

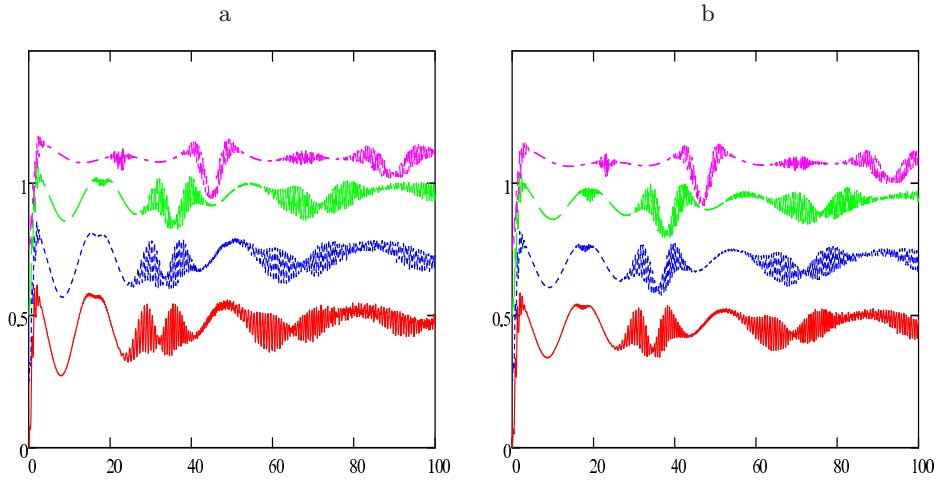

Fig. 1. The time evolution of linear entropy as a function of the scaled time $\lambda_1 t$, with the atoms initially in excited state and the field prepared in a coherent state with fixed amplitude $\alpha = 5$, (a) $\lambda_2 = 0$ and $\delta_1/\lambda_1 = 0.1P(t)$, $\delta_1/\lambda_1 = 3(P(t) + 0.25)$, $\delta_1/\lambda_1 = 5(P(t) + 0.5)$, $\delta_1/\lambda_1 = 10(P(t) + 0.75)$, (b) the same as (a) but for $\lambda_2/\lambda_1 = 4$.

the conclusion that the quantum dynamics associated with the presented atom-field quantum system lead to the entanglement between the atom and the field. On the other hand, the linear entropy of the field is a criterion which implies the strength of entanglement. The higher (lower) the entropy, the greater (smaller) the degree of entanglement. This encouraged us to investigate the time evolution of the entropy for the present system. To study the dynamics of the entanglement, we have to use a suitable measure. For the present case, we use the linear entropy or von Neumann reduced entropy [26]. The linear entropy can be determined from the quantity $P(t) = 1 - \mathrm{Tr}[\hat{\rho}_f^2(t)]$, where $\hat{\rho}_f(t)$ is the field reduced density matrix. A necessary and sufficient condition for the ensemble to be described in terms of a pure state is that $\mathrm{Tr}[\hat{\rho}_f^2(t)] = 1$, in this case a state-vector description of each individual system of the ensemble is possible. For the case $\mathrm{Tr}[\rho_f^2(t)] < 1$ the field will be in a statistical mixture state. However, for a maximally mixed ensemble we have $\mathrm{Tr}[\rho_f^2(t)] = \frac{1}{4}$, because of the diminution of the reduced space in this case for two two-level atoms.

Analytical conclusions about the system state vector dynamics and atom-field entanglement can be reached through the examination of the linear entropy, since a linear entropy of reduced atomic (or field) density matrix can serve for entanglement degree evaluation of the systems consisting of two subsystems and being prepared in a pure state. It is to be mentioned for this special initial pure state that the entropies of the subsystems (atom or field) are equal, according to Araki-Lieb inequality [27]. Therefore, in our investigations we take into account, as stated before, that the atoms are initially in the excited states, *i.e.* $c_1 = 1$ and $c_i = 0$, $i = 2, 3, 4$ in eq. (8) and the field is prepared in a coherent state $|\alpha\rangle$. From eqs. (11) and (14) together with eq. (15) where only A_{11}, A_{21}, A_{31} and A_{41} are nonzero while the rest of the coefficients vanish, it is easy to show that the linear entropy for the atomic state takes the form

$$\begin{aligned} P(t) = 1 &- \left(\sum_{n=0}^{\infty} |X_1(n,t)|^2\right)^2 - \left(\sum_{n=0}^{\infty} |X_2(n,t)|^2\right)^2 \\ &- \left(\sum_{n=0}^{\infty} |X_3(n,t)|^2\right)^2 - \left(\sum_{n=0}^{\infty} |X_4(n,t)|^2\right)^2 \\ &-2\left|\sum_{n=0}^{\infty} X_1(n+1,t)X_2^*(n,t)\right|^2 - 2\left|\sum_{n=0}^{\infty} X_1(n+1,t)X_3^*(n,t)\right|^2 \\ &-2\left|\sum_{n=0}^{\infty} X_1(n+2,t)X_4^*(n,t)\right|^2 - 2\left|\sum_{n=0}^{\infty} X_2(n,t)X_3^*(n,t)\right|^2 \\ &-2\left|\sum_{n=0}^{\infty} X_2(n+1,t)X_4^*(n,t)\right|^2 - 2\left|\sum_{n=0}^{\infty} X_3(n+1,t)X_4^*(n,t)\right|^2 . \end{aligned} \tag{17}$$

The analysis and discussion of the linear entropy is handled through eq. (17). To do so we plot in fig. 1 the function $P(t)$ against the scaled time $\lambda_1 t$. We display the evolution of the linear entropy for different values of the involving

parameters. We have fixed the value of the initial coherent parameter $\alpha = 5$ and in fig. 1a we take $\lambda_2 = 0$, $\delta_1/\lambda_1 = 0.1$ (red solid curve), $\delta_1/\lambda_1 = 3(P(t) + 0.25)$ (dotted blue curve), $\delta_1/\lambda_1 = 5(P(t) + 0.5)$ (green dashed curve) and $\delta_1/\lambda_1 = 10(P(t) + 0.75)$ (purple dot-dashed). In this case we observe that the linear entropy in general satisfies the inequality $0 \leq P(t) \leq 0.6$ as was considered in the fig. 1, where the system approaches the pure state after the onset of the interaction displaying weak entanglement. This means that the state of the field and the atoms are almost at the minimum values of $P(t)$. However, as the time increases the function shows rapid fluctuations with a decrease in its maximum value. Also we note that the rapid fluctuations for the cases $\delta_1/\lambda_1 = 0.1$ and 3 are more pronounced than for the cases $\delta_1/\lambda_1 = 5$ and 10. Furthermore, the function shifts up in the cases $\delta_1/\lambda_1 = 5$ and 10 and oscillations are faster than in the other two cases.

When we take the effect of the coupling parameter into account, such as $\lambda_2/\lambda_1 = 4$, the linear entropy exhibits similar behavior to the previous case. However one can realize that there are slight fluctuations that appear at the maximum value of the second period which is pronounced for $\delta_1/\lambda_1 = 3$ and 5, see fig. 1b. Also we noted that the linear entropy reduces its maximum as well as its minimum. This means that an increase in the value of the coupling between the atoms leads to the reduction in the degree of entanglement beside it gets far from the pure state of the field. The same behavior can be seen when we consider the cases in which $\delta_1 = 0$ or 4 for different values of the coupling parameter λ_2 (not presented here).

4 Atomic characteristics

The atomic inversion represents the difference between the population of the excited and the ground atomic states. In fact using the atomic inversion we can observe the atom in its excited or ground state, and also we can indicate when the atom reaches a super position state. To discuss the atomic inversion we have to calculate the reduced atomic density matrix

$$\hat{\rho}_{\text{atoms}}(t) = \text{Tr}_{\text{field}}|\psi(t)\rangle\langle\psi(t)|, \tag{18}$$

where $|\psi(t)\rangle$ is the time-dependent wave function (11). If we assume that the atom starts in its excited state, the density matrix for a single atom is obtained when we take the trace over one of the atoms, thus we have

$$\begin{aligned} \hat{\rho}_{\text{at(j)}} &= \text{Tr}_{\text{at}(i)}\hat{\rho}_{\text{atoms}}(t),\ i,j = 1,2, \\ \hat{\rho}_{(i)} &= \rho_{11}|+\rangle_{ii}\langle+| + \rho_{12}|+\rangle_{ii}\langle-| + \rho_{21}|-\rangle_{ii}\langle+| + \rho_{22}|-\rangle_{ii}\langle-|, \end{aligned} \tag{19}$$

where

$$\begin{aligned} \rho_{11}(t) &= \sum_{n=0}^{\infty}\left(|X_1(n,t)|^2 + |X_2(n,t)|^2\right),\ \rho_{22}(t) = \sum_{n=0}^{\infty}\left(|X_3(n,t)|^2 + |X_4(n,t)|^2\right), \\ \rho_{12}(t) &= \rho_{21}^*(t) = \sum_{n=0}^{\infty}\left(X_1(n+2,t)X_3^*(n,t) + X_2(n+2,t)X_4^*(n,t)\right). \end{aligned} \tag{20}$$

Since the two atoms are identical, the above equation can well fit for either atom.

The atomic inversion $W(t)$ for one of the atoms takes then the form

$$W(t) = \rho_{11}(t) - \rho_{22}(t). \tag{21}$$

As one can see, it is quite difficult to analyze explicitly the result obtained from the above equation, therefore we plot some figures to display the behavior of the function $W(t)$. For this reason we have used numerical computations to plot the atomic inversion against the scaled time $\tau = \lambda_1 t$. In our investigations we take into account, as stated before, the atoms are initially in the excited states and the field is prepared in a coherent state $|\alpha\rangle$. Furthermore, we have fixed the coherent parameter $\alpha = 5$.

In fig. 2a we plot the atomic inversion for different values of λ_2/λ_1 and in the absence of the detuning δ_1. For instance we consider the case in which $\delta_1/\lambda_1 = 0$ (solid curve) where the atomic inversion shows regular oscillations between the upper and the lower states around zero. As one can see, the phenomenon of revival occurs once after the onset of the interaction for a short period of time. The revival time for this case is $\pi\sqrt{4|\alpha|^2} \simeq 10\pi$ which is twice the revival time for the standard JCM [28], but for $\lambda_2/\lambda_1 \neq 0$ it is $\pi\sqrt{(\lambda_2/\lambda_1)^2 + 4|\alpha|^2}$. This is followed with a long period of collapse, however several periods of the revivals can be seen. In the meantime we observe periods of partial collapses during the considered time. For instance when $\lambda_2/\lambda_1 = 3$ (dotted curve) the behavior is different and one can observe a period of revival with small amplitude during the first collapse period. Moreover, the revivals shift to the right-hand side in addition the partial collapses get more pronounced compared with the previous case. When we consider $\lambda_2/\lambda_1 = 5$ (dashed curve) the function decreases its periods of collapses compared with the previous

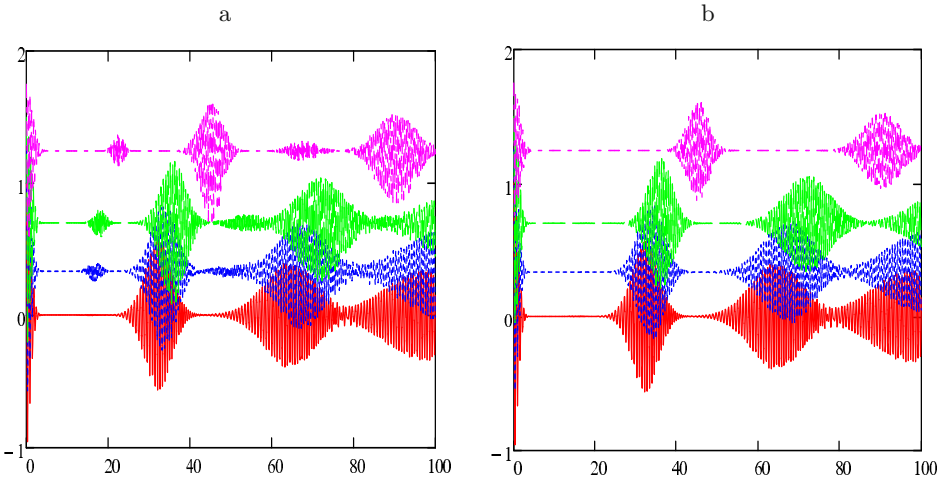

Fig. 2. The time evolution of the atomic inversion as a function of the scaled time $\lambda_1 t$, with the atoms initially in the excited states and the field prepared in a coherent state with fixed amplitude $\alpha = 5$, (a) $\delta_1/\lambda_1 = 0$ and $\lambda_2/\lambda_1 = 0.1, 3, 5, 10$, (b) $\delta_1/\lambda_1 = 0.1W(t)$, $\delta_1/\lambda_1 = 3(W(t) + 0.25)$, $\delta_1/\lambda_1 = 5(W(t) + 0.5)$, $\delta_1/\lambda_1 = 10(W(t) + 0.75)$.

two cases. Also it is observed that when we consider the case in which $\lambda_2/\lambda_1 = 10$ (dot-dashed curve) the function reduces its amplitude during the revivals periods. Also the revivals with smaller amplitudes get more pronounced. These secondary revivals are due to the appearance of the coupling and have times with $2\mu_1(n)t$ as arguments in the trigonometric functions of the coefficients which introduce a revival time of the form $\frac{\pi}{2}\sqrt{(\lambda_2/\lambda_1)^2 + 2|\alpha|^2}$, as in the case of the 3-level JCM [28,29]. Note that the same behavior is seen when we consider $\lambda_2/\lambda_1 > 10$ (not presented here), however the function is only shifted up which means that the coupling parameter plays the role of the detuning parameter. On the other hand, when we consider the case $\lambda_2/\lambda_1 = 0$, while δ_1/λ_1 takes the values $0.1, 3, 5$ and 10, the atomic inversion for all cases fluctuates just above zero. In this case we note that, for a small value of δ_1/λ_1, one can see certain periods of partial collapses, *i.e.* $\delta_1/\lambda_1 = 0.1$, 3, 5 and 10. These periods of partial collapses disappeared and we can only realize the collapses periods, see fig. 2b. Since the revival time is $\pi\sqrt{(\delta_1/\lambda_1)^2 + 4|\alpha|^2}$, we may conclude that for this considerations the parameter δ_1/λ_1 shifts the inversion upward and prolongs the revival time, λ_2/λ_1 does the same but adds the new feature that is attributed to the two-atom interaction.

5 The entropy and variance squeezing

To discuss the quantum fluctuations one can consider the entropy and the variance squeezing which are built on the concept of the uncertainty relations. The argument was to use the entropic uncertainty relations for two-level system rather than the Heisenberg uncertainty relations. This argument has been discussed by the authors of ref. [28,30–36]. It is well known that for a quantum-mechanical system with two physical observables represented by the Hermitian operators $\hat{A}$ and $\hat{B}$ satisfying the commutation relation $[\hat{A}, \hat{B}] = \mathrm{i}\hat{C}$, one can write the Heisenberg uncertainty relation in the form

$$\langle(\Delta\hat{A})^2\rangle\langle(\Delta\hat{B})^2\rangle \geq \frac{1}{4}|\langle\hat{C}\rangle|^2, \tag{22}$$

where $\langle(\Delta\hat{A})^2\rangle = \langle\hat{A}^2\rangle - \langle\hat{A}\rangle^2$. Consequently, the uncertainty relation for a two-level atom characterized by the Pauli operators $\hat{\sigma}_x$, $\hat{\sigma}_y$ and $\hat{\sigma}_z$, satisfying the commutation relation $[\hat{\sigma}_x, \hat{\sigma}_y] = 2\mathrm{i}\hat{\sigma}_z$, can also be written as

$$\Delta\hat{\sigma}_x\Delta\hat{\sigma}_y \geq |\langle\hat{\sigma}_z\rangle|. \tag{23}$$

Note that if $\hat{\sigma}_\alpha$ satisfies the condition

$$V(\hat{\sigma}_\alpha) = \left(\Delta\hat{\sigma}_\alpha - \sqrt{|\langle\hat{\sigma}_z\rangle|}\right) < 0, \quad \Delta\hat{\sigma}_\alpha = \sqrt{\langle\hat{\sigma}_\alpha^2\rangle - \langle\hat{\sigma}_\alpha\rangle^2}, \quad \alpha = x,\ y, \tag{24}$$

then the fluctuations in the component $\Delta\hat{\sigma}_\alpha$ of the atomic dipole is said to be squeezed.

On the other hand, for an arbitrary quantum state the probability distribution for N possible outcomes of measurements of the operator $\hat{\sigma}_\alpha$ is $P_i(\hat{\sigma}_\alpha) = \langle\Psi_{\alpha i}|\hat{\rho}|\Psi_{\alpha i}\rangle$, where $|\Psi_{\alpha i}\rangle$ is an eigenvector of the operator $\hat{\sigma}_\alpha$ such that

$\hat{\sigma}_\alpha|\Psi_{\alpha i}\rangle = \lambda_{\alpha i}|\Psi_{\alpha i}\rangle$, $\alpha = x,\ y,\ z$ and $i = 1,\ 2,\ \ldots,\ N$. The corresponding Shannon information entropies are then defined as

$$H(\hat{\sigma}_\alpha) = -\sum_{i=1}^{N} P_i(\hat{\sigma}_\alpha)\ln P_i(\hat{\sigma}_\alpha),\ \ \alpha = x, y, z. \tag{25}$$

For an N-dimensional Hilbert space, the investigation of the optimal entropic uncertainty relation for sets of $N+1$ complementary observables with nondegenerate eigenvalues can be described by the inequality [37–39]

$$\sum_{k=1}^{N+1} H(\hat{\sigma}_k) \geq \frac{N}{2}\ln\left(\frac{N}{2}\right) + \left(1+\frac{N}{2}\right)\ln\left(1+\frac{N}{2}\right), \tag{26}$$

where $H(\hat{\sigma}_k)$ represents the information entropy of the variable $\hat{\sigma}_k$.

Also it is noted that the uncertainty relation of the entropy can be used as a general criterion for the squeezing in the entropy of an atom, therefore for a two-level atom where $N = 2$, we have $0 \leq H(\hat{\sigma}_\alpha) \leq \ln 2$ and hence from (24), the information entropies of the operators $\hat{\sigma}_x$, $\hat{\sigma}_y$ and $\hat{\sigma}_z$ will satisfy the inequality

$$H(\hat{\sigma}_x) + H(\hat{\sigma}_y) + H(\hat{\sigma}_z) \geq 2\ln 2. \tag{27}$$

In other words, if we define $\delta H(\hat{\sigma}_\alpha) = \exp[H(\hat{\sigma}_\alpha)]$, then we can write

$$\delta H(\hat{\sigma}_x)\delta H(\hat{\sigma}_y)\delta H(\hat{\sigma}_z) \geq 4. \tag{28}$$

It is interesting to mention that the above inequality has been established to be optimal (27), for more details, see refs. [37–39]. The fluctuations in the component $\hat{\sigma}_\alpha$ ($\alpha = x,\ y$) of the atomic dipole are said to be squeezed in entropy if the information entropy $H(\hat{\sigma}_\alpha)$ of $\hat{\sigma}_\alpha$ satisfies the condition

$$E(\hat{\sigma}_\alpha) = \delta H(\hat{\sigma}_\alpha) - \frac{2}{\sqrt{\delta H(\hat{\sigma}_z)}} < 0, \tag{29}$$

where $\alpha = x,\ y$.

To obtain the Shannon information entropies of the atomic operators $\hat{\sigma}_x$, $\hat{\sigma}_y$ and $\hat{\sigma}_z$ for a two-level atom with $N = 2$, one can use the reduced atomic density operator $\hat{\rho}(t)$. Thus we have the following expression:

$$H(\hat{\sigma}_\alpha) = -\frac{1}{2}\left(\rho_\alpha(t)\ln\left[\frac{1+\rho_\alpha(t)}{1-\rho_\alpha(t)}\right] + \ln\left[\frac{1-\rho_\alpha^2(t)}{4}\right]\right),$$
$$\alpha = x, y, z. \tag{30}$$

The time-dependent density matrix is given by

$$\rho_\alpha(t) = \langle\psi(0)|\hat{\rho}_\alpha(t)|\psi(0)\rangle,$$

then from eqs. (19) and (20) we get the expression of the density matrix in the form

$$\rho_x(t) = 2\mathrm{Re}\left[\rho_{12}(t)\right], \quad \rho_y(t) = 2\mathrm{Im}\left[\rho_{12}(t)\right], \quad \rho_z(t) = W(t). \tag{31}$$

We are now in a position to examine the temporal evolutions of the entropy squeezing as well as variances squeezing related to the present system. To do so we plot several figures of the entropy squeezing $E(\hat{\sigma}_x)$ and $E(\hat{\sigma}_y)$ as well as the variance squeezing factors $V(\hat{\sigma}_x)$, $V(\hat{\sigma}_y)$, against the scaled time $\tau = \lambda_1 t$ for the atoms initially prepared in the excited state. Furthermore we have considered the field initially in the coherent state as before.

In fig. 3 we have fixed the value of the amplitude such that $\alpha = 5$ and examined the effect for different values of the involved parameters. For instance we discuss the case in which $\delta_1 = 0$ and $\lambda_2 = 0$ where we observe the squeezing that occurs several times during the considered period of time. In the meantime, the phenomenon of squeezing is pronounced for a short period after the onset of the interaction again. It is also noted that the function displays rapid fluctuations with interference between the patterns. The maximum value of squeezing in this case is carefully checked, and it is found to be -0.356. When we take the effect of the detuning parameter into account, $\delta_1/\lambda_1 = 2$ and $\lambda_2 = 0$, the function $E(\hat{\sigma}_x)$ decreases its value and the squeezing starts to get weaker. It is also observed that when the time increases the value of the squeezing decreases and the value of the maximum squeezing in this case is -0.13, see fig. 3b. When we take the effect of the coupling between the atoms into account, such that $\lambda_2/\lambda_1 = 2$ and ignore the effect of δ_1/λ_1, more decreasing in the amount of squeezing can be seen, see fig. 3c. In this case we can also see more rapid fluctuations building up. Finally when we consider $\delta_1/\lambda_1 = \lambda_2/\lambda_1 = 2$, the phenomenon of squeezing disappeared

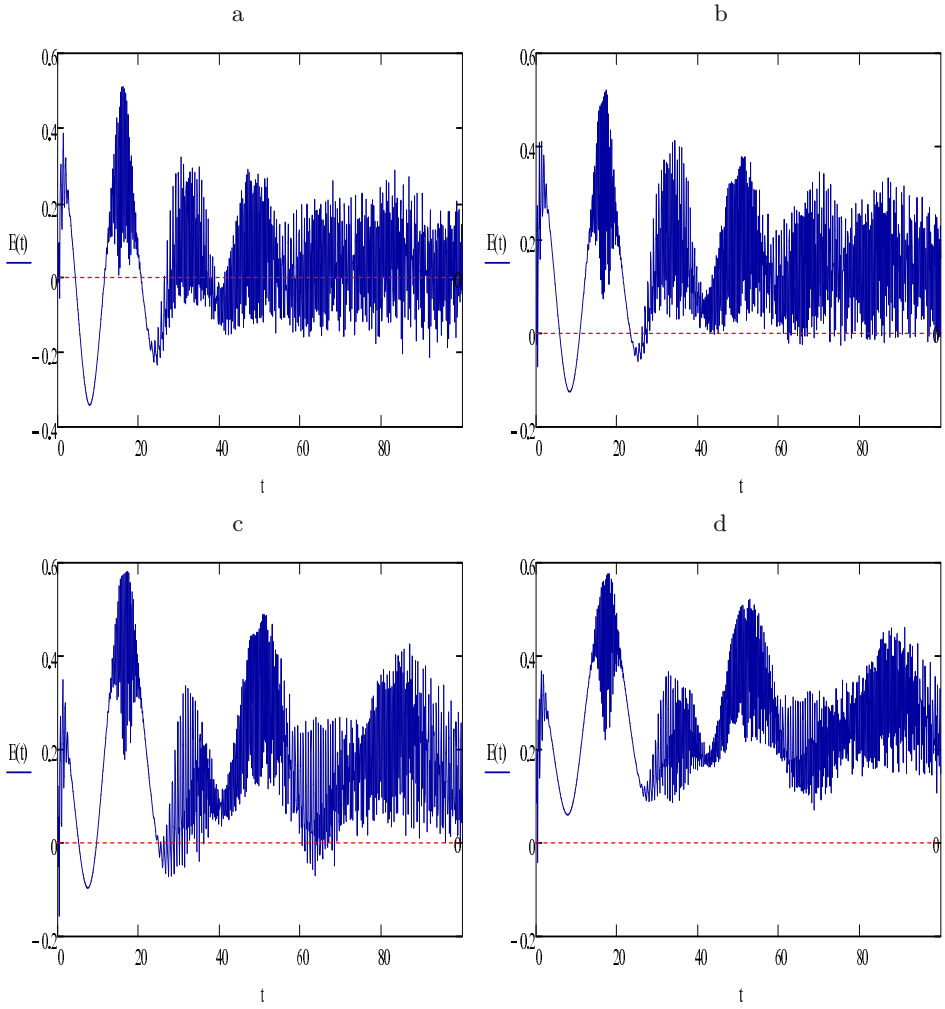

Fig. 3. The time evolution of the entropy squeezing against the scaled time $\lambda_1 t$ where the atoms are initially in the excited states and the field is prepared in the coherent state with the amplitude $\alpha = 5$, (a) δ_1 and λ_2/λ_1 are zero, (b) $\delta_1/\lambda_1 = 2$ and $\lambda_2 = 0$, (c) $\delta_1 = 0$ and $\lambda_2/\lambda_1 = 2$, (d) $\delta_1/\lambda_1 = \lambda_2/\lambda_1 = 2$.

except after the onset of the interaction, however the quadrature still displays rapid fluctuations during the considered period of the time, see fig. 3d.

As soon as we consider the resonance case and neglect the atom-atom interaction, $\delta_1 = 0$ and $\lambda_2 = 0$, it can be seen that the squeezing occurs in three regions during the considered period of time. One can also see that the maximum value of the variance squeezing is less than the entropy squeezing. The maximum squeezing in this case is equal to -0.025. It is also noted that the amount of squeezing in the second period of time is too small compared with the first and third periods of time, see fig. 4(a). When we take the detuning parameter into account, such that $\delta_1/\lambda_1 = 2$ and $\lambda_2 = 0$, the squeezing is increased compared with the previous case and it occurs in two regions, see fig. 4(b). In this case the squeezing gets pronounced, and the quadrature variance shows two different periods where the maximum value of the squeezing occurrs at the value -0.08. On the contrary when we consider the case in which $\delta = 0$ and $\lambda_2/\lambda_1 = 2$, the squeezing behavior is dramatically reduced, however the quadrature variances $V(\sigma_x)$ still displays some squeezing with maximum value at -0.06, see fig. 4(c). Finally a greater increase in the value of the detuning parameter $\delta_1/\lambda_1 = 2$, leads to a decrease in the amount of squeezing, and this occurs only once with maximum value at -0.02, see fig. 4(d). Thus we may conclude that as the value of the coupling between the atoms increases the amount of squeezing decreases. This also depends on the value of the detuning parameter.

6 Pegg-Barnett phase

A Hermitian phase operator in a finite-dimensional state space has been defined by Pegg and Barnett [40–42]. The phase operator is defined as the projection operator on the particular phase state multiplied by the corresponding value

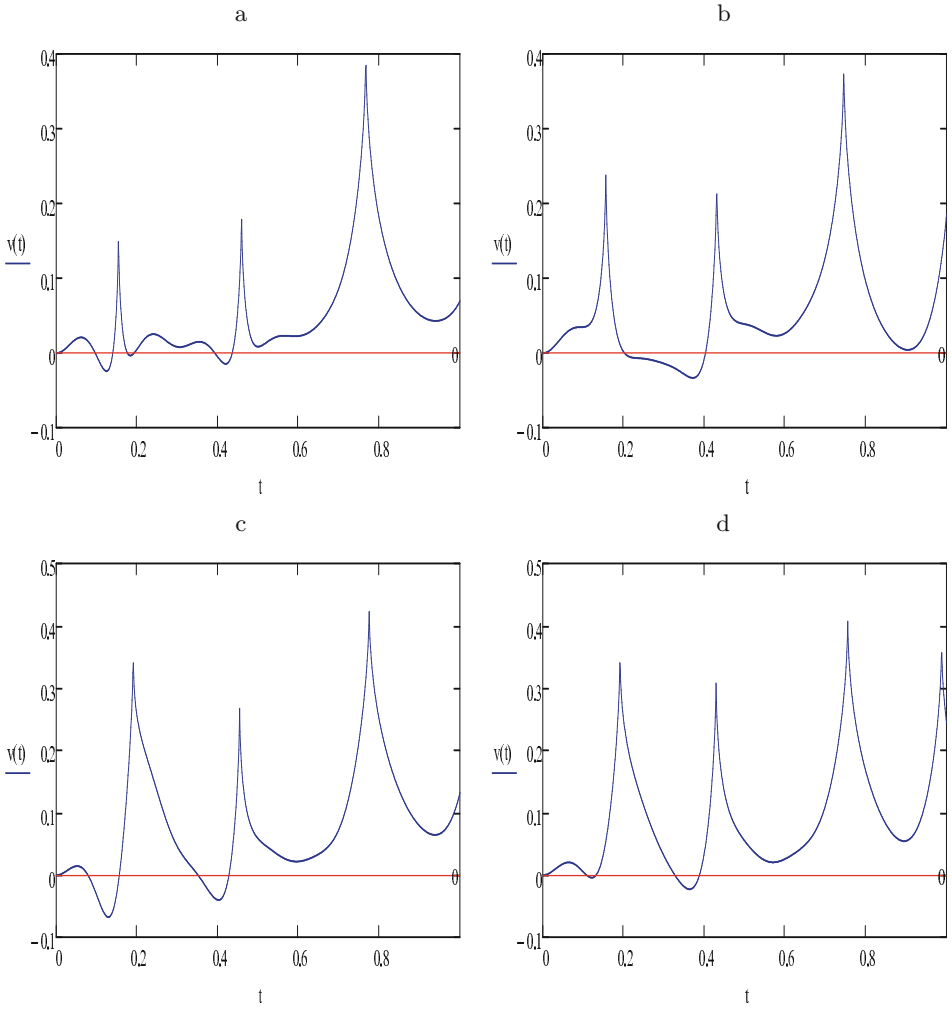

Fig. 4. The time evolution of the variance squeezing against the scaled time $\lambda_1 t$ where the atoms are initially in the excited states and and the field is prepared in the coherent state with the amplitude $\alpha = 5$, (a) δ_1/λ_1 and λ_2/λ_1 are zero, (b) $\delta_1/\lambda_1 = 2$ and $\lambda_2 = 0$, (c) $\delta_1 = 0$ and $\lambda_2/\lambda_1 = 2$, (d) $\delta_1/\lambda_1 = \lambda_2/\lambda_1 = 2$.

of the phase. The main idea of the Pegg-Barnett formalism consists in the evaluation of all expectation values of the physical variables in a finite-dimensional Hilbert space. These give real numbers, which depend parametrically on the dimension of the Hilbert space. Because a complete description of the harmonic oscillator involves an infinite number of states to be taken, a limit is taken only after the physical results are evaluated. This leads to proper limits which correspond to the results obtainable in ordinary quantum mechanics. It can be used for investigating the quantum states phase properties of the electromagnetic-field single mode. Therefore, we will study the phase properties of the Hamiltonian (1) for a coherent state input using the Pegg-Barnett phase formalism. The phase probability distribution is defined by [40–42]

$$\tilde{P}(\theta, t) = \frac{1}{2\pi} \sum_{l,m=0}^{\infty} \rho_{lm}^{f}(t) \exp[\mathrm{i}(l-m)(\theta - \theta_0)], \tag{32}$$

where θ_0 is the phase angle reference which will be ignored in our calculations. The phase distribution, on taking $c_1 = 1$ in eq. (10) and using the field reduced density operator, can be written as

$$\tilde{P}(\theta, \tau) = \frac{1}{2\pi} \left\{ \left| \sum_{n=0}^{\infty} A_{11}(n, \tau) \exp[\mathrm{i}n\theta] \right|^2 + \left| \sum_{n=0}^{\infty} A_{12}(n, \tau) \exp[\mathrm{i}n\theta] \right|^2 + \left| \sum_{n=0}^{\infty} A_{13}(n, \tau) \exp[\mathrm{i}n\theta] \right|^2 + \left| \sum_{n=0}^{\infty} A_{14}(n, \tau) \exp[\mathrm{i}n\theta] \right|^2 \right\}. \tag{33}$$

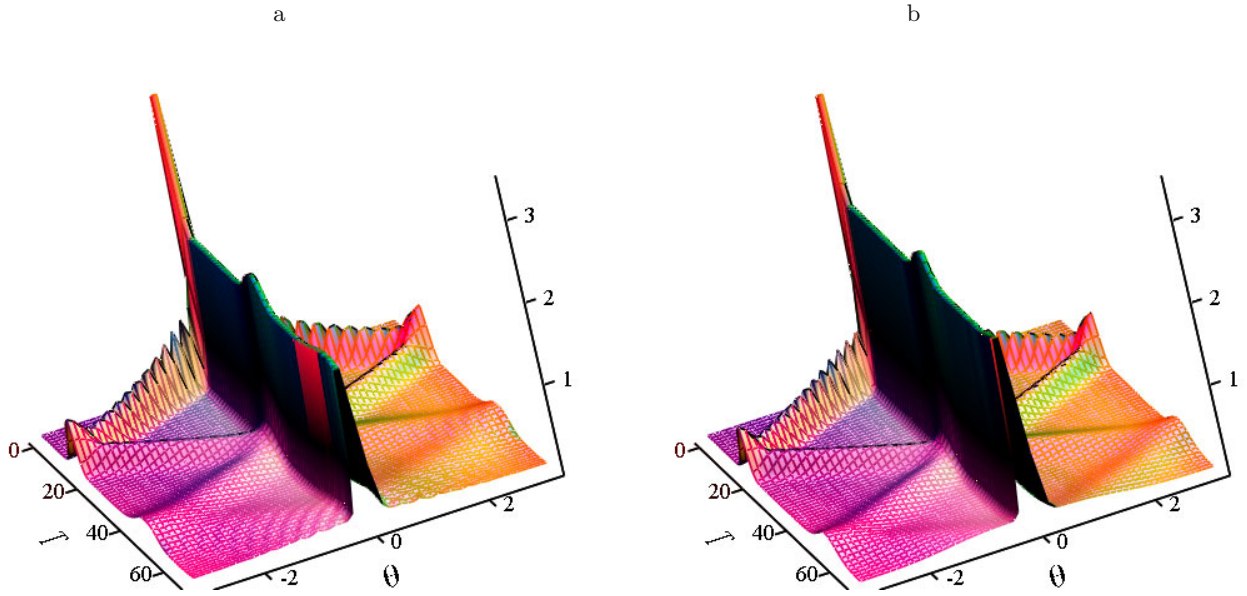

Fig. 5. The Pegg-Barnett phase against the scaled time $\lambda_1 t$ and the phase angle θ where the atoms are initially in the excited states and and the field is prepared in the coherent state with the amplitude $\alpha = 5$, (a) δ_1 and λ_2 are zero, (b) $\delta_1/\lambda_1 = \lambda_2/\lambda_1 = 2$.

To discuss the behavior of the function $\tilde{P}(\theta, \tau)$ we plot fig. 5 against the scaled time τ and the phase angle θ for $\theta \in [-\pi, \pi]$.

Taking $\delta_1/\lambda_1 = 0$ and $\lambda_2/\lambda_1 = 0$ in fig. 5(a), it is seen that at $\tau = 0$ a single peak is observed at $\theta = 0$ but as τ develops, three peaks appear, the one at $\theta = 0$ with large amplitude and two similar side peaks of smaller amplitudes. These two peaks diverge towards $\theta = \pm\pi$ until they reach these values. Thus they occur at mid-revival time as seen in fig. 5(a). But as the time increases further the two side peaks start to converge towards $\theta = 0$ when τ equals the revival time in comparison with the central peak being higher at this point. Increasing time further the two side peaks diverge again but, however, with slightly smaller amplitude compared to the first window appearing when one introduces the amplitude damping [43,44]. When the atomic coupling or the detuning is taken into consideration, the same behavior is displayed with the elongation of the revival time and the lowering of the amplitude of the side peaks, as seen in fig. 5(b).

7 Fidelity

In this section we calculate the fidelity which plays the role of the transition between a pure state $|\psi(0)\rangle$ and the state described by $\hat{\rho}(t) = |\psi(t)\rangle\langle\psi(t)|$. This is equal to the square root of the overlap between the state $|\psi(0)\rangle$ and the state defined by $\hat{\rho}(t)$. The fidelity is given by the form [1],

$$F(t) = \sqrt{\langle\psi(0)|\hat{\rho}(t)|\psi(0)\rangle} = |(\langle\psi(0)|\psi(t)\rangle)|\,. \tag{34}$$

Showing the state close to the initial state due to the initial condition (8) and taking both the atoms in their excited states, we find that the $F(t)$ dependence on $A_{11}(t)$ is symmetric on both δ_1 and λ_2.

Plots of the fidelity for different values of δ_1 and λ_2 are shown in fig. 6. At $\tau = 0$ it attains the value 1 but it sharply drops after $\tau = 0$ to almost a constant value all along the collapse period. Then as in the case of the atomic inversion, however, it builds up towards a peak during the revival period and drops again to the constant value until it reaches a second lower peak at the second main revival. The detuning or the atomic coupling increases the constant value during the collapse period and raises the amplitude of the peaks besides elongation of the collapse period, as indicated in fig. 2b for the atomic inversion. In the meantime, it is noted that the atomic coupling gives the same behavior as the detuning parameter (not presented here). Finally we may point out that the shift between the second and third curves in fig. 2 nearly disappeared in fidelity. This means that the effects of $\delta_1/\lambda_1 = 3$ and 5 are almost the same as for $\lambda_2/\lambda_1 = 4$.

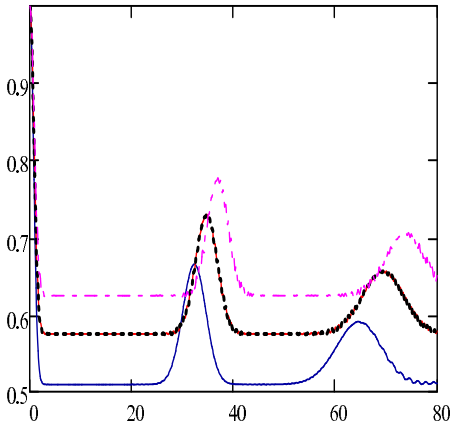

Fig. 6. The fidelity against the scaled time $\tau = \lambda_1 t$, the conditions are the same as in fig. 2b.

8 Field characteristics

In this section we illustrate nonclassical properties of the field in this system using Husimi, Wigner and Glauber-Sudarshan quasidistributions and their variances. Therefore we review basic relations from which we can discuss the effects related to the field.

We have used the wave function (11) to obtain the field density matrix in the form

$$\begin{aligned}\rho_{\text{field}}(t) &= \text{Tr}_{\text{atoms}}|\psi(t)\rangle\langle\psi(t)| \\ &= \sum_{n,m=0}^{\infty} [X_1(n,t)X_1^*(m,t)|n\rangle\langle m| \\ &\quad + X_2(n,t)X_2^*(m,t)|n+1\rangle\langle m+1| \\ &\quad + X_3(n,t)X_3^*(m,t)|n+1\rangle\langle m+1| \\ &\quad + X_4(n,t)X_4^*(m,t)|n+2\rangle\langle m+2|]\,.\end{aligned} \tag{35}$$

Then the Fock density matrix elements are

$$\begin{aligned}\rho(n,m,t) &= \langle n|\rho_{\text{field}}(t)|m\rangle \\ &= [X_1(n,t)X_1^*(m,t) \\ &\quad + X_2(n-1,t)X_2^*(m-1,t) \\ &\quad + X_3(n-1,t)X_3^*(m-1,t) \\ &\quad + X_4(n-2,t)X_4^*(m-2,t)]\,, \\ X_1(n,t) &= X_2(n,t) = X_3(n,t) = X_4(n,t) = 0,\ n<0.\end{aligned} \tag{36}$$

The Husimi quasidistribution $\Phi_A(\alpha,t)$ is then given in [45] (eq. (4.87)), from which the phase-independent quasidistribution $P_A(W,t)$ of the integrated intensity $W = |\alpha|^2$ is obtained.

For the symmetric ordering we have for the Wigner quasidistribution performing the Fourier transformation of the symmetric characteristic function expressed in the Fock states

$$\begin{aligned}\Phi_{\mathcal{S}}(\alpha,t) = \frac{1}{\pi}\sum_{n,m=0}^{\infty}\sum_{k=0}^{n}\sum_{r=\max(0,n-m)}^{\infty} \\ \frac{(-1)^{k+r}\rho(n,m,t)(n!m!)^{1/2}(k+r+m-n)!}{k!(k+m-n)!(n-k)!r!(r+m-n)!} \\ \times 2^{k+r+m-n+1}\alpha^r\alpha^{*r+m-n}.\end{aligned} \tag{37}$$

For computations it is useful to reorganize this expression as follows:

$$\Phi_S(\alpha,t)=\frac{2}{\pi}\sum_{0\le m\le n<\infty}\sqrt{\frac{m!}{n!}}\mathrm{Re}\left[\rho(n,m,t)(2\alpha)^{n-m}\right]$$
$$\sum_{r=0}^{\infty}\frac{(-2|\alpha|^2)^r}{r!}C_{mnr}, \tag{38}$$

where

$$C_{mnr}=a_{mn}\sum_{k=0}^{m}(-2)^k\binom{k+r+n-m}{r+n-m}\binom{n}{m-k},$$
$$a_{mn}=2-\delta_{mn}. \tag{39}$$

The corresponding phase-independent relation is given in [45] (eq. (4.188) for $s=0$). The Glauber-Sudarshan quasidistribution can be obtained as a solution of the moment problem for the photodetection equation as given in [45] eq. (4.113). In an analogous way we obtain the phase-independent Glauber-Sudarshan $P_N(W,t)$, see eq. (3.116) in [45].

9 Illustrations

We can now illustrate the above relations which will really demonstrate nonclassical properties of the field in the interaction with atoms in this system. We assume the initial field in the coherent state with the complex amplitude $\beta=5$ or $\beta=1$ and excited atoms so that $c_1=1$, $c_2=c_3=c_4=0$ as in the earlier sections of this paper. For controlling the numerical results we will use the following relations:

$$\begin{aligned}\langle(\Delta W(t))^2\rangle_{\mathcal{A}} &= \langle(\Delta n(t))^2\rangle+\langle n(t)\rangle+1,\\ \langle(\Delta W(0))^2\rangle_{\mathcal{A}} &= 2|\beta|^2+1,\end{aligned} \tag{40}$$

$$\begin{aligned}\langle(\Delta W(t))^2\rangle_{\mathcal{S}} &= \langle(\Delta n(t))^2\rangle+\frac{1}{4},\\ \langle(\Delta W(0))^2\rangle_{\mathcal{S}} &= |\beta|^2+\tfrac{1}{4},\\ \langle(\Delta W(t))^2\rangle_{\mathcal{N}} &= \langle(\Delta n(t))^2\rangle-\langle n(t)\rangle,\\ \langle(\Delta W(0))^2\rangle_{\mathcal{N}} &= 0.\end{aligned} \tag{41}$$

The averages are taken by means of the corresponding quasidistributions on the left-hand side and by means of the photon number distribution on the right-hand side.

In figs. 7(a), (b), (c) we see the time evolution of the photon number distribution $p(n,t)=\rho(n,n,t)$ for times $t=1$, 3.6, 9.8 ($\lambda_1=1$ as a canonic value, as before, where we choose $\delta_1=0$ (no detuning), $\lambda_2=0$ and $\delta=\delta_1+\mathrm{i}\lambda_2=0$), respectively; and time evolution of the corresponding variances is in fig. 8, both in comparison with the Poisson distribution with the same mean photon number. One can see the successive evolution of the field between sub- and super-Poissonian states.

Adopting the antinormal ordering of field operators, the Husimi quasidistribution and its phase-independent form will exhibit its quantum behavior being narrower or broader than the corresponding initial distributions in correspondence to the variances in (40) and (41):

$$\Phi_{\mathcal{A}}(\alpha,0)=\frac{1}{\pi}\exp(-|\alpha-\beta|^2) \tag{42}$$

and

$$P_{\mathcal{A}}(W,0)=\exp(-W-|\beta|^2)I_0(2(W|\beta|^2)^{1/2}), \tag{43}$$

respectively, I_0 being the modified Bessel function. This is shown in fig. 9 for $t=1.1$ giving the phase-independent Husimi quasidistribution and in fig. 10 showing the time evolution of the variance which periodically increases and decreases the initial value 51. In this case the reduction of the uncertainty in fig. 9 is maximum, as seen in fig. 10. The phase-dependent Husimi quasidistribution is shown in figs. 11(a), (b), (c) for $t=60$, 100, 500 exhibiting quantum oscillations.

Similarly for symmetric ordering we have

$$\Phi_{\mathcal{S}}(\alpha,0)=\frac{2}{\pi}\exp(-|\alpha-\beta|^2) \tag{44}$$

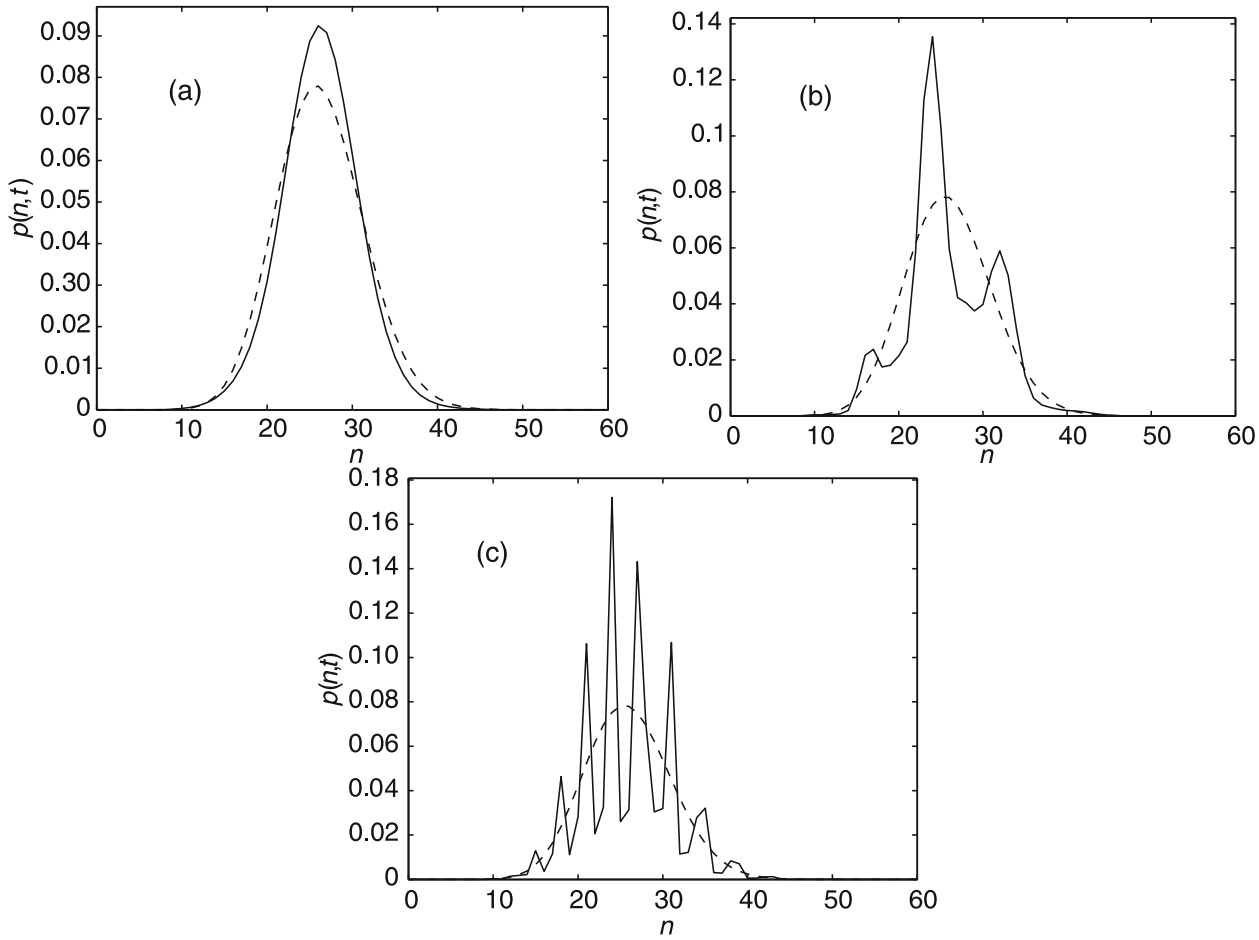

Fig. 7. Photon number distribution $p(n,t) = \rho(n,n,t)$ for (a) $t = 1$, (b) $t = 3.6$ and (c) $t = 9.8$, $\beta = 5$, dashed curve is for Poisson distribution with the same mean photon number.

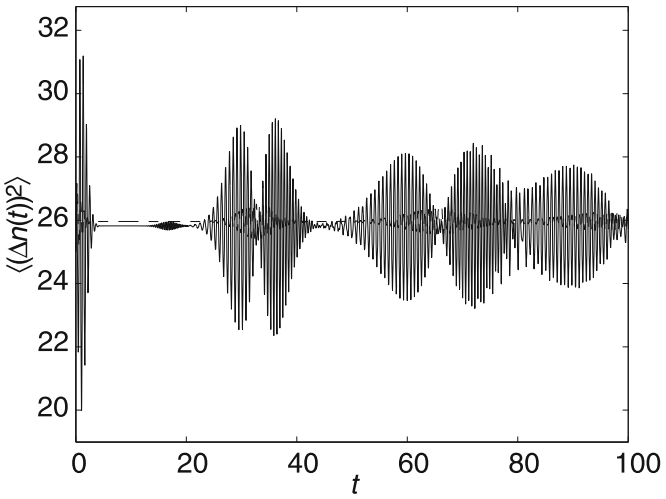

Fig. 8. Time evolution of the corresponding variance $\langle(\Delta n(t))^2\rangle$, $\beta = 5$, dashed curve is for Poisson distribution with the same mean photon number.

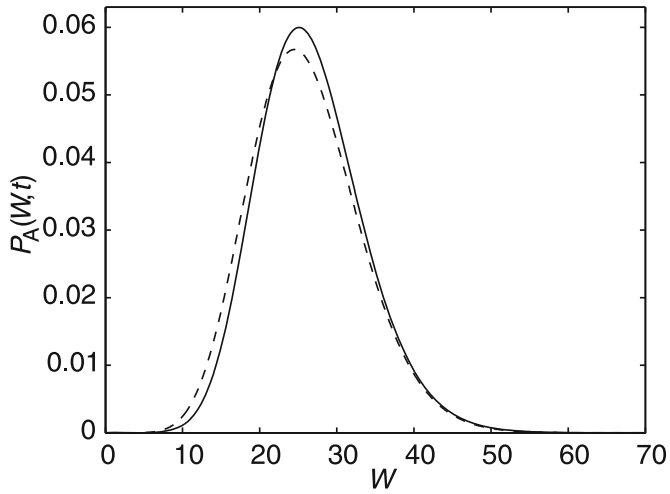

Fig. 9. Phase-independent Husimi quasidistribution $P_{\mathcal{A}}(W,t)$ for $t = 1.1$ and $\beta = 5$, the dashed curve is for the initial distribution with the same mean photon number.

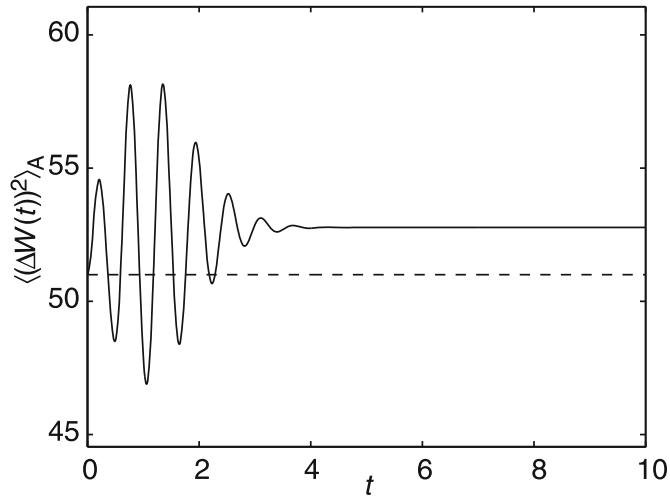

Fig. 10. Time evolution of the corresponding variance $\langle(\Delta W(t))^2\rangle_{\mathcal{A}}$, the dashed line is for the initial distribution with the same mean photon number.

and

$$P_{\mathcal{S}}(W,0) = 2\exp(-W - |\beta|^2) I_0(4(W|\beta|^2)^{1/2}), \tag{45}$$

and the corresponding behavior is in fig. 12 for $t = 6$ exhibiting negative values of the Wigner quasidistribution and the time evolution of the variance for symmetric ordering is in fig. 13 starting at 25.25. For $t = 1.1$ we also obtain the maximum reduction of the uncertainty, as seen from fig. 13, similarly as in fig. 9 for antinormal ordering. Clearly the demonstration of nonclassical behavior is more effective adopting symmetric ordering rather than antinormal ordering. The phase-dependent Wigner quasidistribution computed to test the numerical algorithm for density matrix $\rho_{nm} = \delta_{nm}\delta_{nM}$ (Fock state $|M\rangle$) is seen in fig. 14(a), (b), when $M = 5$ and $M = 10$. Figure 15(a), (b) represent the phase-dependent Wigner quasidistribution for $\beta = 1$ and times $t = 2.5$ and $t = 9.0$ demonstrating clearly its negative values related to the quantum behavior of the system. The highest nonclassical effects can be obtained adopting the normal operator ordering and the corresponding illustration is in fig. 16 for $t = 1$. We clearly see the very rich nonclassical behavior of this quasidistribution. Similar fast quantum oscillations to negative values are obtained in phase-independent Glauber-Sudarshan quasidistribution $P_{\mathcal{N}}(W,t)$ with negative normal variance $\langle(\Delta W(t))^2\rangle_{\mathcal{N}}$ in fig. 17. In general, an increase of detuning δ_1 will reduce the field nonclassical effects, whereas an increase of coupling constant λ_2 of atoms will support them. However, we have verified that the influence of the coupling of atoms on field nonclassical effects is very weak.

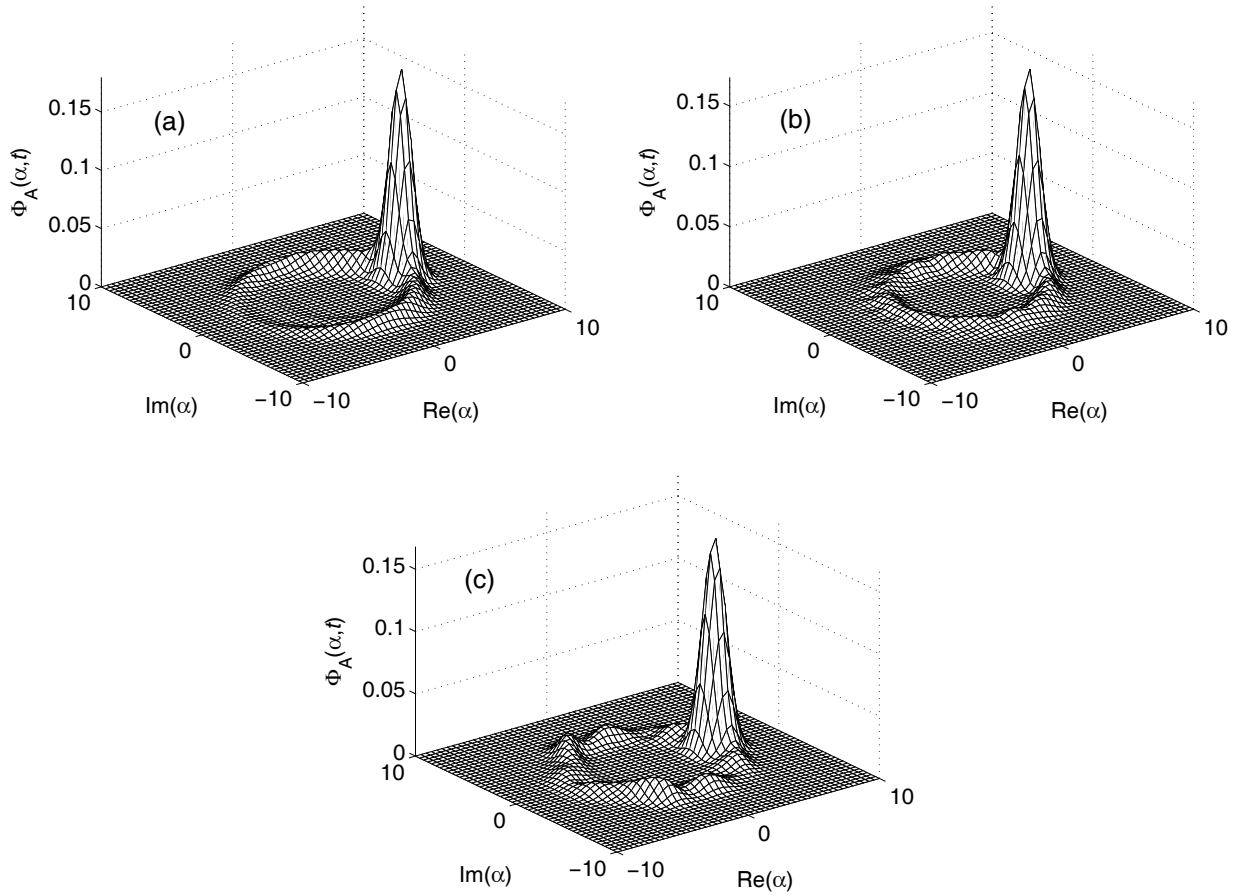

Fig. 11. Phase-dependent Husimi quasidistribution $\Phi_{\mathcal{A}}(\alpha, t)$ for (a) $t = 60$, (b) $t = 100$ (c) and $t = 500$, β as in fig. 1.

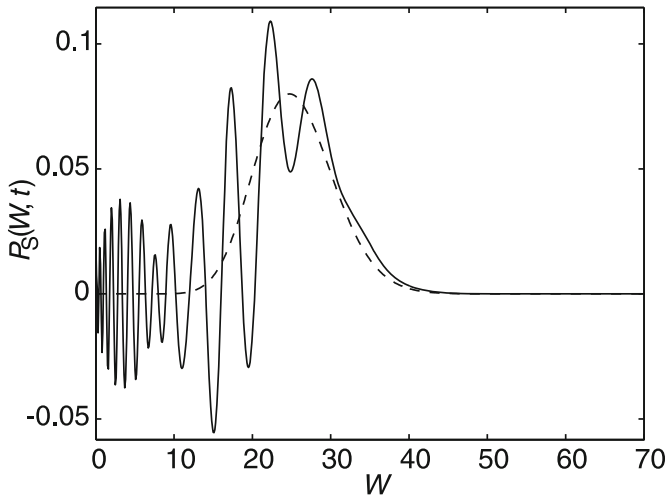

Fig. 12. Wigner quasidistribution $P_{\mathcal{S}}(W, t)$, $t = 6$, β as in fig. 1, the dashed curve is for the initial distribution with the same mean photon number.

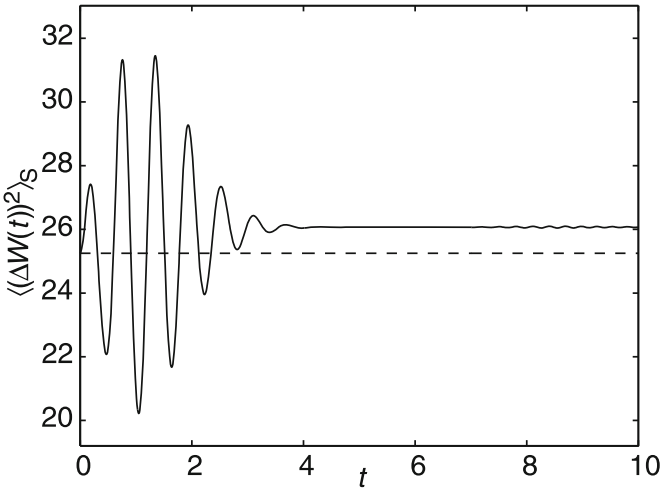

Fig. 13. Time evolution of the corresponding variance $\langle(\Delta W(t))^2\rangle_{\mathcal{S}}$, the dashed line is for the initial distribution with same mean photon number.

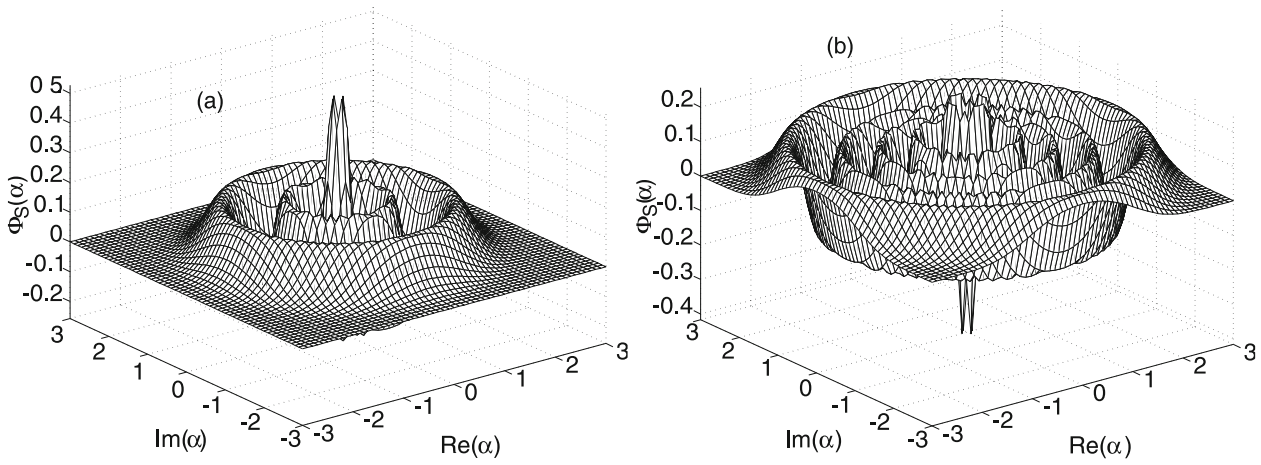

Fig. 14. Wigner quasidistribution $\Phi_{\mathcal{S}}(\alpha,t)$, when $\rho_{nm}=\delta_{nm}\delta_{nM}$ for (a) $M=5$, (b) $M=10$.

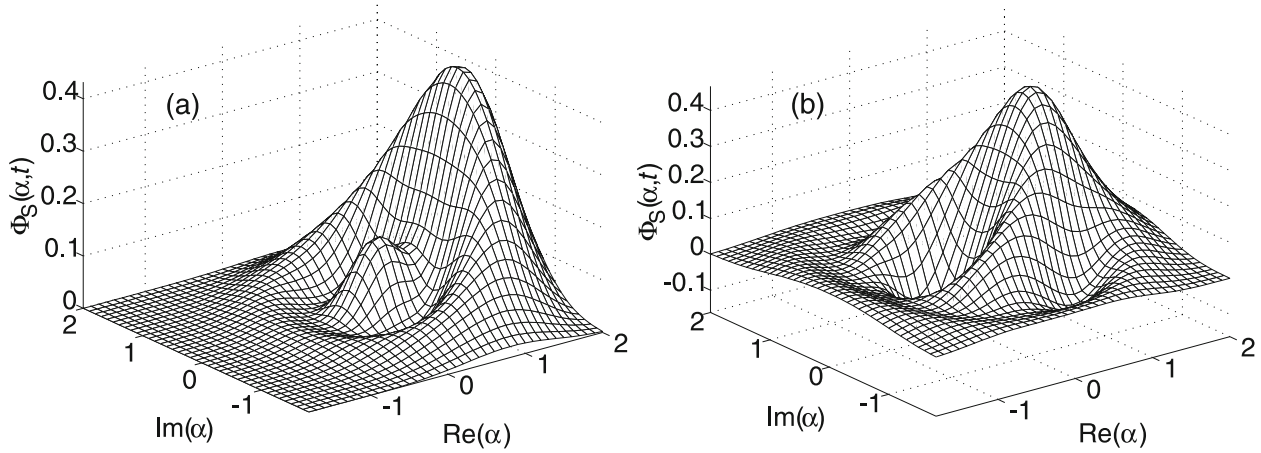

Fig. 15. Wigner quasidistribution $\Phi_{\mathcal{S}}(\alpha,t)$ for $\beta=1$ and times (a) $t=2.5$, (b) $t=9.0$.

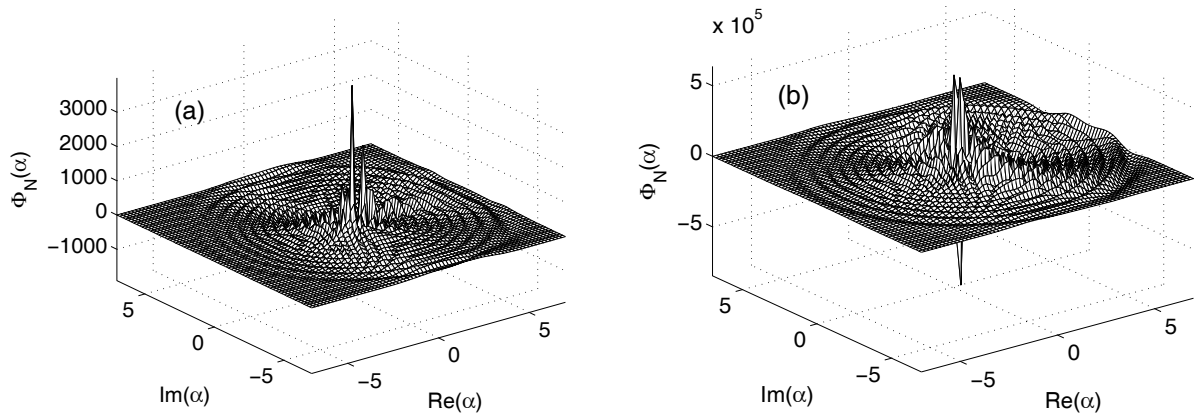

Fig. 16. Glauber-Sudarshan quasidistribution $\Phi_{\mathcal{N}}(\alpha, t)$ for $\beta = 1$ and times (a) $t = 1.0$, (b) $t = 20.0$.

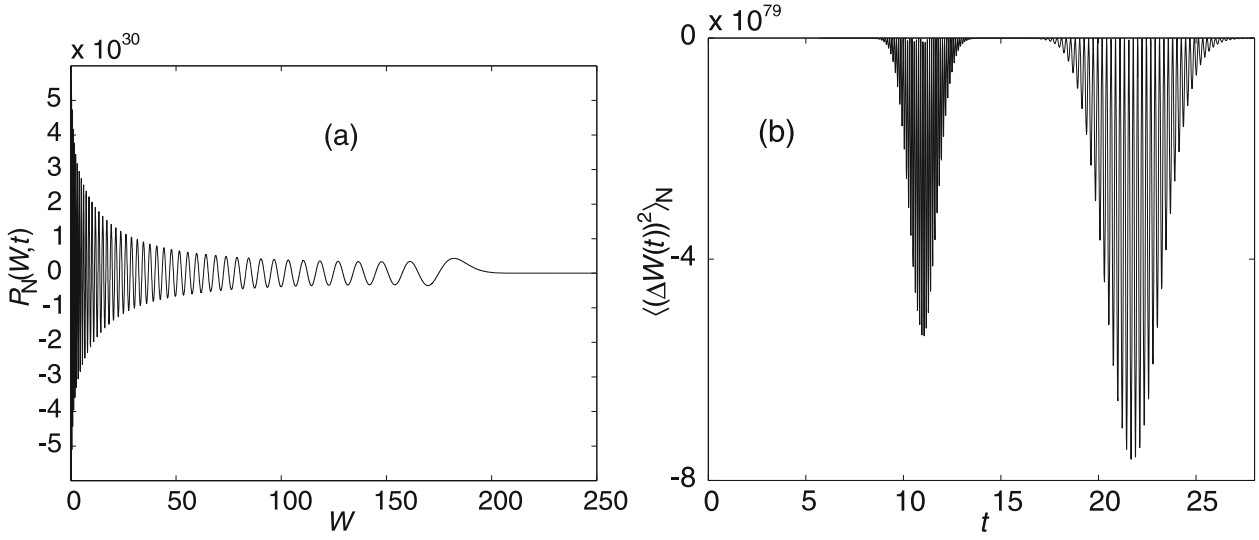

Fig. 17. Glauber-Sudarshan quasidistribution $P_{\mathcal{N}}(W, t)$ (a) for $\beta = 5$ and time $t = 6$ and (b) corresponding normal variance $\langle(\Delta W(t))^2\rangle_{\mathcal{N}}$.

10 Conclusion

In this paper we have considered the problem of the interaction between two two-level atoms and radiation field. The interaction between the atoms is also taken into consideration. The time-dependent wave function is obtained and employed to discuss some statistical properties for the system. For instance, we considered the degree of entanglement using the definition of purity. We found that an increase in the value of the coupling between the atoms leads to a reduction in the degree of entanglement but the function gets further from the pure state. Also we discussed the atomic inversion behavior where the function exhibited periods of revival disappearing in the case in which the detuning parameter δ_1 is zero. We also extended our discussion to include the entropy and variance squeezing. It is showed that the maximum squeezing occurs when $\delta_1 = \lambda_2 = 0$. While for the variance squeezing an increase in the value of the coupling between the atoms leads to observe a greater amount of squeezing. We considered two examples for the Pegg-Barnett phase, for $\delta_1 = \lambda_2 = 0,\ 2$. Similar behavior is observed for both cases except the slight difference in the elongation of the revival time and the lowering of the amplitude of the peak. Finally we considered the normal squeezing, the fidelity, and demonstrated the quantum oscillations of the quasidistributions.

MSA extends his appreciation to the Deanship of Scientific Research at KSU for funding the work through the research group project No. PRG/1436/22. JP and JK thank the support from project LO1305 of the Ministry of Education, Youth and Sports of the Czech Republic.

References

1. M.A. Nielsen, I.L. Chuang, *Quantum Computation and Quantum Information* (Cambridge University Press, Cambridge, 2000).
2. D. Bouwmeester, A. Ekert, A. Zeilinger (Editors), *The physics of quantum information* (Springer, Berlin, 2000).
3. R.G. DeVoe, R.G. Brewer, Phys. Rev. Lett. **76**, 2049 (1996).
4. Q.A. Turchette, C.S. Wood, B.E. King, C.J. Myatt, D. Leibfried, W.M. Itano, C. Monroe, D.J. Wineland, Phys. Rev. Lett. **81**, 3631 (1998).
5. E. Hagley, X. Maitre, G. Nogues, C. Wunderlich, M. Brune, J.M. Raimond, S. Haroche, Phys. Rev. Lett. **79**, 1 (1997).
6. M. Tavis, M. Cummings, Phys. Rev. **170**, 379 (1968).
7. A.S.-F. Obada, Z.M. Omar, J. Egypt Math. Soc. **1**, 63 (1993).
8. I.K. Kudryavtsev, A. Lambrecht, H. Moya-Cessa, P.L. Knight, J. Mod. Opt. **40**, 1605 (1994).
9. H.T. Dung, N.D. Huyen, J. Mod. Opt. **41**, 453 (1994).
10. M. Brune, J.M. Raimond, P. Goy, L. Davidovich, S. Haroche, Phys. Rev. Lett. **59**, 1899 (1987).
11. E.K. Bashkirov, M.S. Rusakova, Opt. Commun. **281**, 4380 (2008).
12. E.K. Bashkirov, Phys. Scr. **82**, 015401 (2010).
13. H.A. Hessian, M. Hashem, Quantum Inf. Process **10**, 543 (2011).
14. D. Bra, Phys. Rev. Lett. **89**, 277901 (2002).
15. F. Benatti, R. Floreanini, M. Piani, Phys. Rev. Lett. **91**, 070402 (2003).
16. S. Oh, J. Kim, Phys. Rev. A **74**, 062306 (2006).
17. M.S. Kim, Jinhyoung Lee, D. Ahn, P.L. Knight, Phys. Rev. A **65**, 040101 (2002).
18. L.M.K. Vandersypen, I.L. Chuang, Rev. Mod. Phys. **76**, 1037 (2004).
19. Y. Makhlin, G. Schön, A. Shnirman, Rev. Mod. Phys. **73**, 357 (2001).
20. R. Loudon, P.L. Knight, J. Mod. Opt. **34**, 709 (1987).
21. S.J.D. Phoenix, P.L. Knight, Phys. Rev. A **44**, 6023 (1991).
22. C.Z. Wang, C.X. Li, G.C. Guo, Eur. Phys. J. D **37**, 267 (2006).
23. M. Abdel-Aty, M.S. Abdalla, B.C. Sanders, Phys. Lett. A **373**, 315 (2009).
24. B. Ghosh, A.S. Majumdar, N. Nayak, Phys. Rev. A **74**, 052315 (2006).
25. R.F. Werner, *Quantum Information – An Introduction to Basic Theoretical Concepts and Experiments*, Springer Tracts Modern Phys., Vol. **173** (Springer, Heidelberg, 2001).
26. S.J.D. Phoenix, P.L. Knight, Phys. Rev. A **44**, 6023 (1991).
27. H. Araki, E. Lieb, Commun. Math. Phys. **18**, 160 (1970).
28. H.I. Yoo, J.H. Eberly, Phys. Rep. **118**, 239 (1981).
29. A.M. Abdel-Hafez, A.S.F. Obada, M.M.A. Ahmed, Phys. Rev. A **35**, 1634 (1987).
30. E.M. Khalil, M.S. Abdalla, A.S.-F. Obada, J. Perina, J. Opt. Soc. Am. B **27**, 266 (2010).
31. E.M. Khalil, M.S. Abdalla, A.S.-F. Obada, J. Phys. B **43**, 095507 (2010).
32. P.L. Knight, P.M. Radamore, Phys. Lett. A **90**, 342 (1982).
33. E.M. Khalil, Int. J. Mod. Phys. B **30**, 5143 (2007).
34. A.-S.F. Obada, M.M.A. Ahmed, F.K. Faramawy, E.M. Khalil, Chaos Solitons Fractals **28**, 983 (2006).
35. M.S. Abdalla, E.M. Khalil, A.S.-F. Obada, Ann. Phys. (N.Y.) **11**, 2554 (2007).
36. E.M. Khalil, M.S. Abdalla, A.S.-F. Obada, Ann. Phys. (N.Y.) **321**, 421 (2006).
37. J. Sanchez-Ruiz, Phys. Lett. A **201**, 125 (1995).
38. J. Sanchez-Ruiz, Phys. Lett. A **244**, 189 (1998).
39. J. Sanchez-Ruiz, Phys. Lett. A **173**, 233 (2003).
40. S.M. Barnett, D.T. Pegg, Phys. Rev. A **19**, 3849 (1986).
41. S.M. Barnett, D.T. Pegg, Phys. Rev. A **39**, 1665 (1989).
42. S.M. Barnett, D.T. Pegg, J. Mod. Optics **36**, 7 (1989).
43. A.S.F. Obada, A.M. Abdel-Hafez, M. Abdel-Aty, Eur. Phys. D **3**, 289 (1998).
44. A.S.F. Obada, A.M. Abdel-Hafez, A.H. Essawy, M. Abdel-Aty, Phys. Scr. **60**, 329 (1999).
45. J. Peřina, *Quantum Statistics of Linear and Nonlinear Optical Phenomena* (Kluwer, Dordrecht, 1991).